Comparison of Measured Stratospheric OII with Prediction

f]. M. Pickett and D. B. Peterson
Jet Prepulsion Laboratory, California Institute of Technology

Short title: STRATOSPHERIC OII

Abstract. The production and loss of stratospheric OH involve relatively fast reactions that are in near photochemical equilibrium. In this study, we compare OH measured by our t)alloon-borne Far Infrared Limb Observing Spectrometer (FILOS) with that predicted from a simple model that uses water and ozone fields obtained from instruments on the Upper Atmosphere Research Satellite (UARS). This comparison is made for latitudes near 34N over a full diurnal cycle for five balloon flights that span a period of over two years. The ratio of measurement to the photochemical model at 40 km is 0.96 with an uncertainty of 0.05 due to the measurement. Comparison at other altitudes and as a function of the diurnal cycle also snow excellent agreement.

Introduction

Since the recognition of human impact on the atmosphere, the stratosphere **has** become an important focus of scientific investigation. Anthropogenic effects on ozone depletion mechanisms have been particularly important because of possible accompanying effects on climate and increased incidence of skin cancer. The HO_x radicals, OH and HO_2 play critical roles in all cycles of ozone destruction. However, the chemistry of HO_x is an uncertain area of stratospheric chemistry. In the chlorine cycle, OH is critical in returning HCl to chlorine atoms. In the nitrogen cycle, tile HO_x radicals play a complex role in the cycling between reservoir species and the active NO and NO_2 radicals. In addition, OH is the major oxidant for methane, SO_2, and the hydrogen-containing chloro-fluorocarbons ($HCFC$) in the stratosphere. Fortunately, the cone.elltrat,ion of the HO_x radicals are governed by fast photochemistry involving water and ozone. 'Thus, concentrations of the HO_x radicals can be implied from a small subset of photochemical reactions with little direct influence of dynamics. On the other hand, secure knowledge of the HO_x concentrations is essential to understanding the other chemical cycles where OH and HO_2 are participants.

Remote sensing instrumentation for measurement of the HO_x radicals has been very challenging. The Upper Atmosphere Research Satellite (UARS) has a number of instruments that can measure ozone and water, as well as key radicals in the chlorine and nitrogen cycles of ozone destruction. However, remote sensing measurements of OH were not sufficiently mature at the time of UARS instrument selection. Since then we have developed the Far Infrared Limb Observing Spectrometer (FILOS), which is a balloon-borne instrument measuring thermal limb emission of OH at 101.3 cm^{-1} and 118.2 cm^{-1} using a triple Fabry-Perot interferometer [*Pickell and Peterson*, 1994]. In addition to FILOS, remote sensing of OH from balloon can be made with lidar [*Heaps and McGee*, 19S5] ant] with Fourier Transform Spectrometers [*Traub et al.*, 1988; *Park and Carli, 1991*].

Column measurements from the ground and in situ measurements complement remote sensing measurements of HO_x. Column OH has been measured extensively from the ground using a Fabry-Perot instrument at *308.2* nm [*Burnett and Burnett*, 19S3]. This provides a good time history from a limited set of locations. While very useful as a stand alone instrument, it would be helpful to compare columns obtained with this technique with altitude resolved observations from space. in situ measurements of OH and HO_2 using ultraviolet resonant fluorescence of OH have been performed by the Anderson group at Harvard from balloon [*Stimpfle et al.*, 1990] and aircraft [*Salawitch et al.*, 1994]. Measurements by this technique are valuable for determining OH in the lower stratosphere, where the far infrared instruments have reduced sensitivity because of water vapor absorption.

'There have been a number of attempts Lo estimate OH globally using satellite

measurements of other species. Satellite measurements of HNO_3 and NO_2 have been used to derive OH from LIMS observations [*Pyle et al.*, 1983] by assuming pilot.ochemical equilibrium in production and loss of HNO_3. Another approach is to assume photochemical equilibrium for sources and sinks of HO_x and then to use satellite measurements of ozone, water, and other relevant species to infer OH. This has been used by two groups [*Pyle and Zavody*, 1985; *Kaye and Jackman*, 1986] to estimate OH using LIMS and SAMS observations.

In this paper we will describe a simplified photochemical model for OH which uses ozone and water measurements from instruments on UARS. Results from this model will be compared with data from FILOS for latitudes near 34N over a full diurnal cycle for five balloon flights that span a period of over two years.

Chemical Model

The photochemical model we use is based on production of OH by reaction of water and methane with O(* 1)) and by direct photolysis of water. Destruction of HO_x (OH +HO_2 -i H) is primarily by reaction of OH with HO_2, although reaction of OH with nitric acid, which *converts* HO_x to NO=, is included. The photolysis and reaction steps used are given in 'Table 1. The CH_3 radical produced in the last two reactions is assumed to be oxidized to formaldehyde with a unit yield of HO_2. However, photolysis of formaldehyde and other minor sources of HO_x are not included.

Photochemical equilibrium of O atom production and loss gives $[O(^1D)] = J_1[O_3]/k_1[M]$ and $[O] = J_2[O_3]/k_4[O_2][M]$. The steady-state equation for the production and loss of HO_x is

$$\{k_2[O(^1D)] + J_3\}[H_2O] + k_{15}[O(^1D)][CH_4]$$
$$- k_{11}[HNO_3][OH] - k_3[HO_2][OH] = 0 \qquad (1)$$

where assumption of steady-state for HNO_3 has been used to eliminate the dependence on J_4 and k_{14}. Consideration of steady-state rate equations for $[HO_2]$ and $[H]$ leads to a pair of algebraic equations which can be solved to give:

$$c_1[HO_2] = c_2[OH] - c_3[H_2O] \qquad (2)$$

where

$$c_1 = k_8[O] + k_9[O_3] + k_{10}[NO] \qquad (3)$$

$$c_2 = fk_5[O] + k_6[O_3] + fk_7[CO] \qquad (4)$$
$$+ k_{11}[HNO_3] + k_{16}[CH_4]$$

$$c_3 = (1 - f)J_3 - i\,k_2[O(^1D)] \qquad (5)$$

$$f = \frac{k_{13}[O_2][M]}{k_{12}[O_3] + k_{13}[O_2][M]} \qquad (6)$$

Table 1. Reactions for OH Model

O_3	+	$h\nu$			→	$O(^1D)$	+	O_2	J_1
O_3	+	$h\nu$			→	O	+	O_2	J_2
H_2O	+	$h\nu$			→	OH	+	H	J_3
HNO_3	+	$h\nu$			→	OH	+	NO_2	J_4
$O(^1D)$	+	M			→	O	+	M	k_1
$O(^1D)$	+	H_2O			→	$2\ OH$			k_2
OH	+	HO_2			→	H_2O	+	O_2	k_3
O	+	O_2	+	M	→	O_3	+	M	k_4
OH	+	O			→	H	+	O_2	k_5
OH	+	O_3			→	O_2	+	HO_2	k_6
OH	+	CO			→	H	+	CO_2	k_7
HO_2	+	O			→	OH	+	O_2	k_8
HO_2	+	O_3			→	OH	+	$2\ O_2$	k_9
HO_2	+	NO			→	OH	+	NO_2	k_{10}
OH	+	HNO_3			→	H_2O	+	NO_3	k_{11}
H	+	O_3			→	OH	+	O_2	k_{12}
H	+	O_2	+	M	→	HO_2	+	M	k_{13}
OH	+	NO_2	+	M	→	HNO_3	+	M	k_{14}
$O(^1D)$	+	CH_4			→	OH	+	CH_3	k_{15}
OH	+	CH_4			→	H_2O	+	CH_3	k_{16}

Note that f is the fraction of Ii atom reactions that produce HO_2 and is close to unity below 80 km. The final solution for [OH] is obtained by substituting Eq.(2) into Eq.(1) and finding the positive root of the resulting quadratic equation. It might appear that Eq.(2) could lead to negative concentrations of HO_2, but the form of the solution is such that this never happens for positive rate constants and concentrations.

Inclusion of chlorine chemistry would not change the HO_x production and loss in Eq.(1), since there is **no** net consumption of HO_x. Under normal conditions, we do not expect that this extra chemistry will modify the partitioning of HO_x between OH and HO_2. In fact, in much of the stratosphere, this partitioning is dominated by the leading terms in the expression for c_1 and C_2.

The rate constants are taken from the NASA pane] for kinetic data evaluation [*DeMore et al.*, 1994]. The most difficult part of the model calculation is determining the J values, which involves integrating photochemical yields, solar irradiance, and opacity over wavelengths of 175-850 nm. We use the solar irradiance and absorption of ozone and oxygen from Chap. 7 of the WMO report [*WMO*, 1985]. Calculation of the oxygen opacity includes contributions from the Herzberg and Schumann-Runge bands. Water absorption and $O(^1 D)$ photochemical yields are taken from the kinetic data evaluation [*DeMore et al.*, 1994]. The total opacity calculations include contributions for the curvature of the Earth. Corrections for multiple Raleigh scattering are made using a six stream **model** [*Prather, 1993*] and assuming a surface albedo of 30%. The surface albedo correction has significance only for the visible wavelength contribution to J_2, which only influences the altitude where the OH/HO_2 ratio becomes dominated by the O atom concentration.

Under most circumstances, the dominant contribution to the photochemical model comes from reactions that involve water and ozone. Therefore, concentrations for HNO_3, NO, CO, and methane are fixed at climatological values typical for a latitude of 34N. A more refined use of the model could include measured values for these molecules, but since their contributions represent corrections to the dominant effects of water and ozone, the error in using fixed values should be small.

This model was compared with results presented at the 1992 NASA Models and Measurements Workshop [*Nasa Ref. Publ. 1292*, 1993]. Our results for $J(O(^1 D))$, O density, $O(^1 D)$ density, OH density, and HO_2 density were virtually indistinguishable from the other models.

Experimental Measurements

The balloon measurements of OH reported here were obtained on five flights in the southwest United States near 34 N latitude. Particulars of these flights are given in 'l'able 2. The pressure range listed is the atmospheric pressure (in mbar) at the gondola.

Remote stratospheric measurements of OH arc very challenging because of the strongly inverted OH concentration profile. For more evenly distributed species most of the emission comes from atmospheric layers near the tangent height. In contrast, for OH much of the emission near the line center comes from higher levels. However, Letter tangent. level concentrations can be obtained by moving slightly off emission line center, where the lower altitude OH is pressure broadened into the instrument pros-band. in fact, the derivative of the emission with respect to low altitude OH has a maximum away from line center due to opacity near the line center. From space, OH vertical concentration profiles with altitude can be made from approximately 20--80 km. The lower limit comes from absorption by water and the upper limit comes from the decrease in OH concentration in the high mesosphere. For balloo1]-based observations, the information about concentrations above the altitude of the balloon is more limited due to observational geometry.

The procedures for calibration and retrieval have been described in a previous publication [*Pickett and Peterson,* 1994]. Recently, two additional calibration issues were discovered which significantly affect the quality of the results. They arc (1) determination of the effective resolution of the scanning l'abry-l'trot etalon and (2) determination of the center frequency of the intermediate resolut ion F'abry-Perot etalon which acts as the blocking filter for orders of the scanning etalon.

Determination of the resolution of the FILOS scanning etalon at 101.3 cm^{-1} has always been determined by measurement of 1 I DO in a sample cell at pressures between 0.6 mbar and 5 mbar. Then the apparent cone.cntration in the sample cell is retrieved as a function of pressure using different, assumed resolutions. We have consistently obtained a full width at half maximum of 0.0016 cm^{-1} at this frequency with an estimated uncertainty of 8%. Recently, we applied the same procedure to the 118.2 cm^{-1} channel using NH$_3$ as the calibration gas. For the retrieval we used the recently determined self-broadening widths for NH$_3$[*Brown and Peterson,* 1994]. Surprisingly, the resultant etalon width is 0.0027 cm^{-1}, which is considerably larger than a previous estimate which assumed that the resolution was linear with frequency. This new value for the effective resolution increases the OH concentrations retrieved from the 118.2 cm^{-1} channel by nearly 30% and makes the OH concentrations retrieved from the two OH channels identical to within experimental error. In this work, we have applied this new resolution value retroactively to all previous measurements that used the 118.2 cm^{-1} channel.

The center frequency of the intermediate resolution etalon is determined by mounting the entire cryostat on our Bruker 120 spectrometer in one of the detector positions. It is critical for this measurement to align the optical axis of the Bruker interferometer with the optical axis of the cryostat. Previously, we performed the alignment by maximizing the detected far infrared power at the detector. This procedure has proved to be inadequate, especially when the blocking filter is not exactly centered on the OH lines.

Our new procedure is to replace the usual polyethylene window on the cryostat with a z-cut crystal quartz window and to align the focal aperture on the liquid He cold surface with the visible light from the Hg arc source from the spectrometer. This procedure was validated at 118.2 cm^{-1} using the N 113 measurements described above. When the center frequencies based on the new procedure are used, the retrieved NH_3 concentration was 1.003:0.07 volume mixing ratio. The NH_3 measurement is particularly sensitive because the lines arc on the edge of the blocking filter.

Correction of the data from earlier balloon flights is made difficult because the filter etalons have been adjusted on occasion to improve their performance. Fortunately, the 118.2 cm^{-1} channel etalons have not been modified from the beginning of 1993 until the time of the improved measurements. The 101.3 cm^{-1} channel etalons have been modified, but there is a signature in the calibration which reliably indicates the center of the filter etalon. This signature is a sinusoidal component of the black body calibration signal which is clue to the fact that a different amount of black body light reaches the detector when an order of the scanning Fabry-Perot etalon is centered on the peak of the blocking filter than when the orders straddle the filter. We therefore use the phase of this component of the calibration signal to determine the center frequency in the historical record. The shape of the blocking filter for tile higher frequency channel is such that the amplitude of this calibration signature is greatly diminished and is unreliable. In the special case of our September 1992 data, we adjusted the position of the 118.2 cm^{-1} filter center frequency so as to make the 011 concentration the same for both channels when averaged over all altitudes and over the entire flight. This gave us lower noise levels over shorter time intervals, but the data for the two channels is not completely independent.

The OH concentrations for all the flights were retrieved using a common functional form. Below the balloon, the data were fitted to a distribution which was piecewise linear in number density with vertices separated by factors of 2.15 in pressure ($\sim$5 km intervals) beginning at the gondola atmospheric pressure level. For the region from 2.5 km above the balloon to approximate] y 90 km, the OI I concentration was scaled to the photochemical model using UARS temperature, water, and ozone profiles. OH concentrations for the intermediate 2.5 km region were linearly interpolated in number density from the sample point at the balloon altitude and the assumed shape above the balloon. Low altitude OH was constrained by an assumed *a priori* OH profile which was equal to the values predicted by the model with an uncertainty equal to the value of noon-time OH model prediction. The actual retrieval involved an iterative least squares fit to all the data in a selected 30--60 minute time period. As an aid in inter-comparison, the retrieved 011 concentrations and the uncertainties from the fit are reported on a standard pressure level grid, thereby compensating for altitude changes during tile flight.

Comparisons

The comparison of observed OH with model predictions was made for each of the five flights. The temperature, water and ozone fields for the model are obtained from UARS data. Data from the Microwave Limb Sounder (MLS) on UARS were used for the first two flights, while data from the Halogen Occultation Experiment (HALOE) were used for the last three flights. The latitude match for each of the data sets was within 2.5 degrees, while the longitude mismatch was a large as 1 0 degrees. MLS data were taken from the same day as the flight, while HALOE data were taken from the day of best latitude match (which differed by as much as 5 days from the day of the balloon flight).

The solar zenith angles used for the model period were derived from the actual latitude and longitude of the balloon during the integration period along with the latitude and longitude of the sub-solar point. The the actual solar zenith angle along a given line of sight is also dependent on the heading. For example, if the line of sight is north at local noon, the solar zenith angle at a tangent height of 30 km is 2.5° less than the solar zenith angle at the gondola.. However, for the purposes of the present comparison, the solar zenith angle at the gondola is used. A more refined comparison would also require that the retrieval account for gradients in OH along the line of sight. Currently, we assume a spherically symmetric concentration distribution for the retrieval, i.e. no concentration gradients along the line of sight, as do virtually all limb retrieval algorithms.

The diurnal behavior of OH at 3.2 mbar is shown in Figure 1 and 2. While the nominal pressure level is 3.2 mbar, this level is actually representative of the scaled distribution at higher altitude, as discussed above. However, sensitivity analysis has shown us that FILOS is not particularly sensitive to OH above 60 km, because the OH emission lines are optically thick and emission at higher altitudes is absorbed by OH between 40 and GO km. 'The slight irregularities in the Sept. 1993 model profile are due to small latitude changes during the flight, which began near local noon and extended into the next day. The diurnal behavior of OH at 10 mbar is shown in Figures 3 and 4. For both pressure levels, the shape of the observed diurnal variation is consistent with the model. However, the May data at 10 mbar appears to be lower than the model by 25%.

The correlation between the model and the observations is shown more directly in Figures 5 and 6. The solid lines are present as a guide in viewing the correlation and have no further significance. The numerical results from fitting the **Slopes of such** correlation curves is shown in 'Table 3. The data at 3.2 mbar show little variation from flight to flight, and the ratio shows very good agreement between observations and the model. The data at pressures near 10 mbar has more scatter, and the differences are correlated with season. The February data have the highest ratios, the May data have

lowest ratios, and the September data have ratios in the middle and close to unity.

As an aid in comparing the FILOS measurements with ground-based column measurements of OH, we have calculated the column density above 25 km. This quantity is calculated directly in our fitting program, and includes an uncertainty estimate based on the full covariance of the fit. The diurnal variations arc shown in Figure 7 and 8. The right axis shows the air mass (secant of the solar zenith angle) for the corresponding local time. The differences bet wccn observation and the model just after sunset arc due to OH above 50-60 km where the chemistry is not likely to be in photochemical equilibrium. The model uses the correct geometry that accounts for the later sunset at higher altitudes, but does not account for any time lag in the disappearance of the OH. This high altitude OH makes a bigger contribution just after sunset because the foreground OH has already disappeared. The correlation plot of OH column in Figure 9 shows that the column is not very sensitive to the seasonal differences observed near 10 mbar. As can be seen from the last row in Table 3, the ratio of the experimental column to the model is unity within experimental error.

Conclusions

At altitudes of 40 km and above, or pressures lower than 3.2 mbar, the average ratio of observed to model OH is 0.96 with an uncertainty of 0.05 due to the observations. At these altitudes, the OH concentration is approximately proportional to $\sqrt{[O_3][H_2O]}$. The estimated uncertainty in the satellite measurement is 5 % for ozone and 10 % for water, leading to 5 % uncertainty in the model OH from these **sources**. The uncertainty in the rates also affect the absolute accuracy of the OH model, **but. the** estimation of errors is complicated by likely correlation between the reaction rates. For example, the ratio k_2/k_1 should be Letter known than the individual values. A critical rate constant for the OH mode] is the rate for HO_x loss, k_3. The uncertainty in k_3 at 250 K is currently 48 %, **which** leads to an uncertainty of 22 % in the OH concentration. Errors in J_1 and in the solar flux will also produce uncertainty in the model which is approximately half as large as the input errors. Therefore, the observed OH is in excellent agreement with the model OH, especially considering the uncertainties in both the observations and the model. The observed OH is also consistent with other measurements rnadc with lidar [*Heaps and McGee,* 19S5], with Fourier Transform Spectrometers [*Traub et al.,* 19S8; *Park and Carli,* 1991], and with in situ measurements of OH using ultraviolet resonant fluorescence [*Stimpfle et al.,* 1990]. However, because of differences in the solar zenith angle as well as seasonal differences in ozone and water, it is difficult to compare the the measurements to a level which is consistent with the experimental error. During several of the balloon flights, FILOS has shared the gondola with cach of the two far infrared Fourier Transform Spectrometers. Results of this comparison will be the subject of a

Table 2. FILOS Balloon Flights

Date	Latitude	Longitude	Pressure (mbar)
2/20/92	36.8 --37.1	251.5 --258.0	2.9–3.3
9/29/92	34.6 --35.8	256.8 --259.8	3.7-5.1
5/31/93	34.4 --34.9	253.2 --255.7	3.s-10.
9/25/93	32.3-34.5	256.9--259.9	4.0-4.9
5/15/94	34. S-35.S	254. S--255.S	4.1-6.2

Table 3. Ratio of Observed OH /Model OH

Pressure (mbar)	5/94	9/93	5/93	9/92	2/92	Average
21.5	0.55 ± 0.36	0.80 ± 0.57	0.87 ± 0.10	1.36 ± 0.41	1.47 ± 3 9 3 0 - 9 1 9 1	± 0.09
14.7	0. 69 ± 0.15	0.95 ± 0.25	0. 89 ± 0.11	1.16 ± 0.26	1 . 6 4 ± 0.49	0. 89 ± 0.08
10.0	0 . 7 4 ± 0.12	0.99 ± 0.23	0.7 8 ± 0.15	1 . 0 4 ± 0.24	1.75 ± 0.33	0.88 ± 0.06
4.6	0.82 ± 0.11	0. 87 ± 0.19	0.72 ± 0.22	0.93 ± 0.10	1 . 2 4 3 , 0 . 1 6	0.92 ± 0.06
3.2	0.96 ± 0.10	1.02 ± 0.11	0.79 ± 0.29	0.93 ± 0.10	0.97 ± 0.13	0.96 ± 0.05
col umn	0.92 ± 0.10	1 . 0 4 ± 0.11	0.92 ± 0.37	0 . 9 4 ± 0.10	0 . 9 4 ± 0.13	0.96 ± 0.05

forthcoming paper.

Our data for the OH column is also in excellent agreement with the photochemical model. This column is the integral of OH number density OH above 25 km along a vertical pat h. The contribution to the OH column can be estimated using observed values for ground level OH [*Mount and Eisle,* 1992]. Using a midrange value of $2 \times 10^6 cm^{-3}$ and an effective tropospheric OH scale height of 11 km, the tropospheric contribution to the column is $0.22 \times 10^{13} cm^{-2}$. The noon value for total vertical OH **column** for the May 1994 flight (air mass = 1.05) is therefore $6.0 \pm 0.6 \times 10^{13} cm^{-2}$. This number is consistent with columns measured from the ground in the 1977-1979 period, but not with more recent measurements [*Burnett et al.,* 1989]. As discussed above, the 1"11.0S measurements are not sensitive to mesospheric OH or tropospheric OH. However, for the model OH profile, the tropospheric **contribution to the vertical column** is less than 4 % of tile total and the contribution of OH above 60 km is 25 %. Therefore, a change of OH column from $6 \times 10^{13} cm^{-2}$ to 10×10^{13} cm^{-2}, as observed by *Burnett et al.,* 1989, would require a 367% increase in the mesospheric OH. The FILOS flight in September 1993 is the only flight, of tile set of five flights, where both morning and afternoon arc available. As can be seen from Figure 7, there is a hint of a negative AM-PM asymmetry which is most pronounced near air mass = 3. However, this asymmetry can easily be attributed to a '20 min lag in the photochemistry. Such a lag is consistent with the time scale for the OH production and loss reactions.

The observed seasonal effects are potentially very interesting but *more work* needs to be done both in tile modeling and in observations to understand the effect. Near 10 mbar, the OH mixing ratio changes a factor of two with a change in altitude of 2.5 km. Therefore, very subtle effects in the measurement **or** the model could influence the height, registration and lead coincidently to the 25% difference observed between the May and September data.

References

Brown, L. R., **and** D. B. Peterson, An empirical expression for linewidths of ammonia from far-infrared measurements, *J. Molec. Spectrosc. 168*, 593-606, 1994.

Burnett, C. R., and E. B. Burnett, OH Pepsios, *Appl. Optics*, 22, '2287- 2892, 1983.

Burnett, E. D., C. R. Burnett, and K. R. Minschwaner, Periodic behaviors in the observed vertical column n abundances of atmospheric hydroxyl, *Geophys. Res. Lett., 16*, 1285--1288, 1989.

DeMore, W. B., S. P. Sander, D. M. Golden, R. F. Hampson, M. J. Kurylo, C. J. Howard, A. R. Ravishankara, C. E. Kolb, and M. J. Molina, Chemical kinetics and photochemical data for use in stratospheric modeling: evaluation number 11, *JPL Publication 94-26*, 1994.

Heaps, W. S., and T. J. McGee, Progress in stratospheric hydroxyl measurements by balloon-borne lidar, *J. Geophys. Res.*, 90, '7913--7922, 1985.

Kaye, J. A., C. H. Jackman, Concentrations and uncertainties of stratospheric trace species inferred from Limb infrared Monitor of the stratospheric data, *J. Geophys. Res., 91*, 1117-1135, 1986.

Mount, G. H. and F. L. Eisele, An inter-comparison of tropospheric OH measurements at Fritz Peak Observatory, Colorado, Science 256, 1187--1190, 1992.

Park, J. H., and B. Carli, Spectroscopic measurement of HO_2, H_2O_2, and OH in the stratosphere, *J. Geophys. Res., 96*, 22,535-22,.541, 1991.

Pickett, H. M., and D. B. Peterson, Stratospheric OH measurements with a far-infrared limb observing spectrometer, *J. Geophys. Res.*, 98, 20,507–20,515, 1993.

Prather, M. J., GISS photochemical model, *NASA Ref. Publ. 1292, Vol. I* 76-80, 1993.

Prather, M. J., and E. E. Remsberg, Eds., *NASA Ref. Publ. 1292, Vol. III*, 1993.

Pyle, J. A., A. M. Zavody, J. E. Harries, and P. H. Moffat, Derivation of OH concentration from satellite infrared measurements of NO_2 and HNO_3, *Nature* 305, 690-692, 1983.

Pyle, J. A., and A. M. Zavody, The derivation of hydrogen-containing radical concentrations from satellite data sets, *Quart. J. R. Met. Sot., 111*, 993--1012, 1985.

Stimpfle, R. M., P. O. Wennberg, L. B. Labson and J. G. Anderson, Simultaneous in situ measurements of OH and HO_2 in the stratosphere, *Geophys. Res. Letters, 17*, 1905-1908, 1990.

Salawitch, R. J., S. C. Wofsy, P. O. Wennberg, R. C. Cohen, J. G. Anderson, D. W. Fahey, R. S. Gao, E. R. Keim, E. L. Woodbridge, R. M. Stimpfle, J. P. Koplow, D. W. Kohn, C. R. Webster, R. D. May, L. Pfister, E. W. Gottlieb, H. A. Michelsen, G. K. Yue, J. C. Wilson, C. A. Brock, H. H. Jonsson, J. E. Dye, D. Baumgardner, M. H. Proffitt, M. Loewenstein, J. R. Podolske, J. W. Elkins, G. S. Dutton, E. J. Hintsa, A. E. Dessler, E. M. Weinstock, K. K. Kelley, K. A. Boering, B. C. Daube, K. R. Chan, and S.

W Bowen , The distribution of hydrogen, nitrogen, and chlorine radicals in the lower stratosphere: Implications for changes in O_3 due to emission of NO_y from supersonic aircraft, *Geophys. Res. Letters,* 23, 2547-2550, 1994.

Traub, W. A., D.G. Johnson, and K. V. Chance, Stratospheric hydroperoxyl measurements, *Science, 247,* 446--449, 1990.

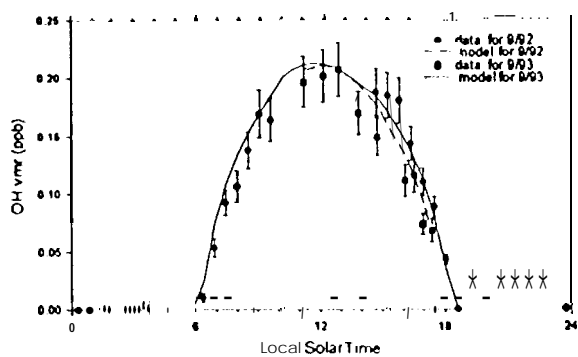World Meterological Organization, Atmospheric ozone 1985, *Global Ozone Research* and *Monitoring Project, Report16,* 1095.

Figure 1. September OH at 3.2 mbar
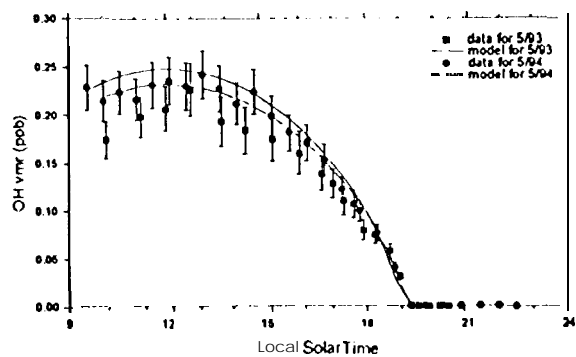
Figure 2. May OH at 3.2 mbar
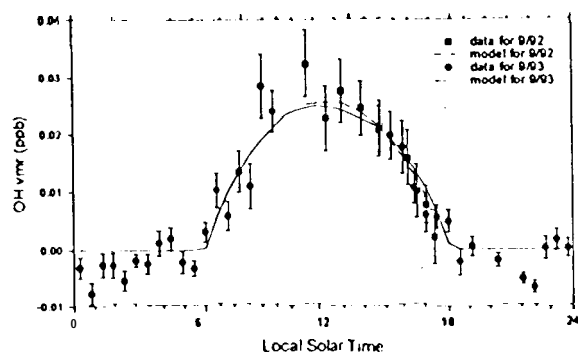
Figure 3. September OH at 10 mbar
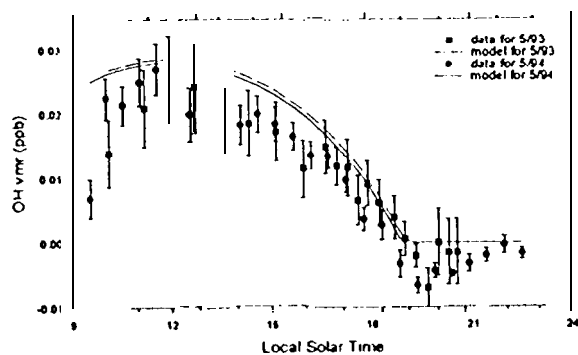
Figure 4. May OH at, 10 mbar
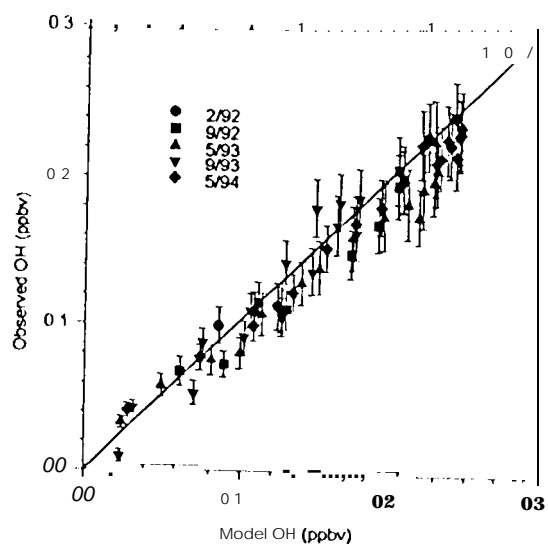
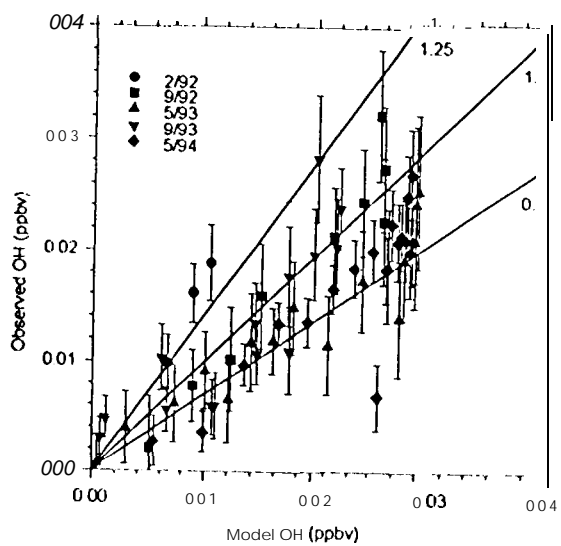Figure 5. OH correlation at 3.2 mbar

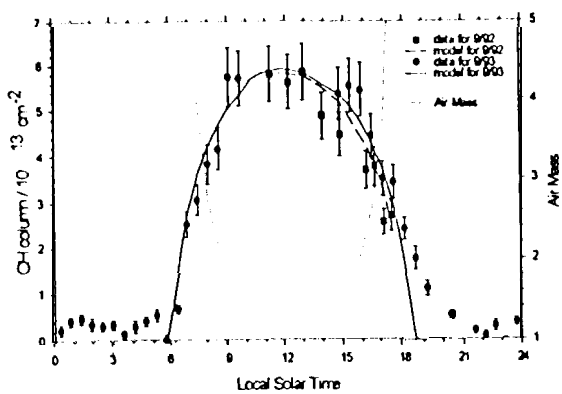
Figure 6. OH correlation at 10 mbar
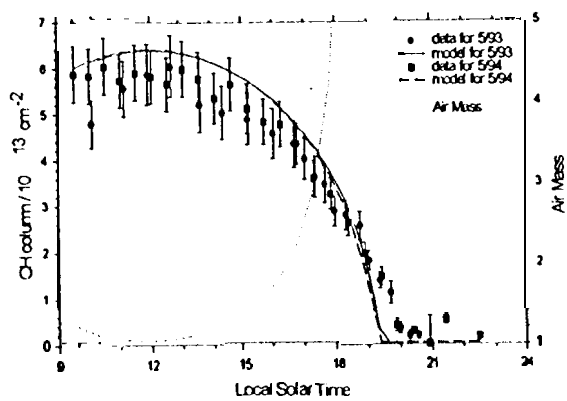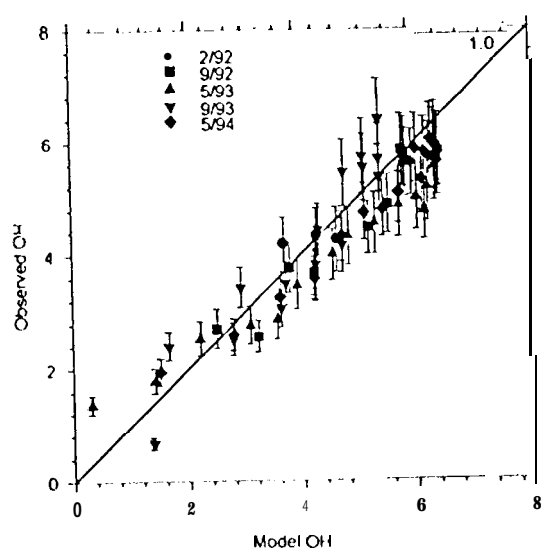
Figure 7. September vertical 011 column

Figure 8. May vertical 011 column

Figure 9. OH column correlation